arXiv:1701.08964v1 [cond-mat.mes-hall] 31 Jan 2017

Enhancing Photon Correlations through Plasmonic Strong Coupling

R. Sáez-Blázquez,[1] J. Feist,[1] A. I. Fernández-Domínguez,[1,*] and F. J. García-Vidal[1,2,†]

[1]*Departamento de Física Teórica de la Materia Condensada and Condensed Matter Physics Center (IFIMAC), Universidad Autónoma de Madrid, E- 28049 Madrid, Spain*

[2]*Donostia International Physics Center (DIPC), E-20018 Donostia/San Sebastián, Spain*

We investigate the quantum statistics of the light scattered from a plasmonic nanocavity coupled to a mesoscopic ensemble of emitters under low coherent pumping. We present an analytical description of the intensity correlations taking place in these systems, and unveil the fingerprint of plasmon-exciton-polaritons in them. Our findings reveal that plasmonic cavities are able to retain and enhance excitonic nonlinearities even when the number of emitters is large. This makes plasmonic strong coupling a promising route for generating nonclassical light beyond the single emitter level.

Much research attention has focused lately on nanocavities for strong coupling applications. In these devices, the interaction between surface plasmons (SPs) and quantum emitters (QEs) can be intense enough to yield new hybrid light-matter states, the so-called plasmon-exciton-polaritons (PEPs) [1]. PEPs involving macroscopic QE ensembles have been reported in planar [2–4] and nanoparticle [5–7] geometries, and they have been used for controlling chemical reactions [8, 9] or enhancing charge/energy transport [10, 11]. From a purely photonics perspective, room temperature PEP lasing has been recently reported [12]. However, in order to fully harness the potential of plasmonic cavities for optical applications, quantum nonlinearities must be retained [13]. This is not possible in macroscopic ensembles, which present collective boson-like behavior at pumping levels below the QE saturation regime [14].

Very recently, strong-coupling signatures in the power spectrum of nano-gap metallic cavities filled with only a few QEs have been reported [15, 16]. These experimental advances have been accompanied by theoretical efforts aiming to clarify the near-field conditions yielding PEPs at the single emitter level [17]. However, the generation of nonclassical light through plasmonic strong coupling has not been explored yet. In this Letter, we fill this gap by investigating the quantum statistics of the photons scattered by a nanocavity strongly coupled to a mesoscopic emitter ensemble (up to ~ 100 QEs) under coherent pumping. We develop an analytical description of the quantum optical properties of the system that allows us to reveal that, contrary to what is expected, plasmonic cavities allow photon correlations to survive in QE ensembles of considerable size under strong coupling conditions.

Figure 1 depicts the system under study: N identical QEs with transition dipole moment $\boldsymbol{\mu}_{\rm QE}$ and frequency $\omega_{\rm QE}$ interact with the near-field $\mathbf{E}_{\rm SP}$ (the same for all QEs) of a single SP mode of energy $\omega_{\rm SP}$ supported by a generic nanocavity. Both subsystems undergo radiative and nonradiative damping, with decay rates $\gamma_{\rm QE/SP} = \gamma^{\rm r}_{\rm QE/SP} + \gamma^{\rm nr}_{\rm QE/SP}$, and are coherently driven by a laser field $\mathbf{E}_{\rm L}$ with frequency $\omega_{\rm L}$. The steady-state density matrix $\hat{\rho}$ for the hybrid system

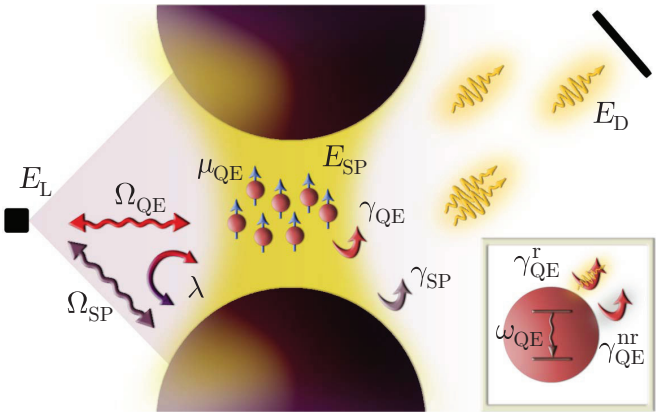

FIG. 1. A QE ensemble resonantly coupled to a generic plasmonic cavity. The set of parameters characterising the system are sketched. The right inset depicts the two-level QE model.

is the solution of the Liouvillian equation

$$\frac{i}{\hbar}[\hat{\rho},\hat{H}]+\frac{\gamma_{\rm SP}}{2}\mathcal{L}_{\hat{a}}[\hat{\rho}]+\frac{\gamma^{\rm r}_{\rm QE}}{2}\mathcal{L}_{\hat{S}^-}[\hat{\rho}]+\frac{\gamma^{\rm nr}_{\rm QE}}{2}\sum_{i=1}^{N}\mathcal{L}_{\hat{\sigma}_i}[\hat{\rho}]=0, \tag{1}$$

where $\hat{a}$, $\hat{\sigma}_i$, and $\hat{S}^- = \sum_{i=1}^{N}\hat{\sigma}_i$ are the annihilation operators for the SP mode, the i-th QE, and the ensemble superradiant state, respectively. The damping associated to operator $\hat{O}$ is described by standard Lindblad super-operators $\mathcal{L}_{\hat{O}}[\hat{\rho}] = 2\hat{O}\rho\hat{O}^\dagger - \{\hat{O}^\dagger\hat{O},\rho\}$. In the rotating frame, the coherent dynamics is governed by the time-independent Tavis-Cummings Hamiltonian [18]

$$\begin{aligned}\hat{H} = \hbar\Delta_{\rm SP}\hat{a}^\dagger\hat{a} + \hbar\Delta_{\rm QE}\hat{S}_z + \hbar\lambda(\hat{S}^+\hat{a}+\hat{S}^-\hat{a}^\dagger) + \\ +\hbar\Omega_{\rm SP}(\hat{a}^\dagger+\hat{a}) + \hbar\Omega_{\rm QE}(\hat{S}^+ + \hat{S}^-),\end{aligned} \tag{2}$$

with $\Delta_{\rm QE/SP} = \omega_{\rm QE/SP} - \omega_{\rm L}$ and $\hat{S}_z = \frac{1}{2}[\hat{S}^+,\hat{S}^-]$. The QE-SP coupling is $\lambda = \mathbf{E}_{\rm SP}\cdot\boldsymbol{\mu}_{\rm QE}$, while $\Omega_{\rm QE} = \mathbf{E}_{\rm L}\cdot\boldsymbol{\mu}_{\rm QE}$ and $\Omega_{\rm SP} = \mathbf{E}_{\rm L}\cdot\boldsymbol{\mu}_{\rm SP}$ are the pumping amplitudes. Here, $\boldsymbol{\mu}_{\rm SP}$ is the effective SP dipole moment. Once the steady-state density matrix is known, the first- and second-order correlation functions can be calculated from the scattered far-field operator at the detector $\hat{\mathbf{E}}^-_{\rm D} \propto \boldsymbol{\mu}_{\rm SP}\hat{a}^\dagger + \boldsymbol{\mu}_{\rm QE}\hat{S}^+$.

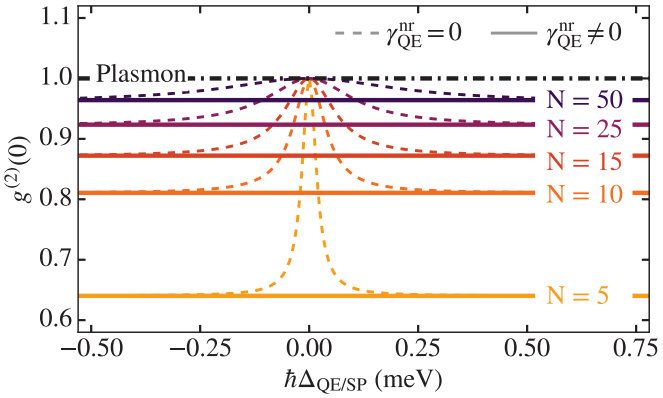

FIG. 2. Zero-delay second-order correlation function versus laser detuning for SP (black dash-dotted line) and QEs (color lines) uncoupled. Various ensembles sizes are shown, with (solid) and without (dashed) the inclusion of QE nonradiative decay, γ_{QE}^{nr}.

Before investigating photon correlations under strong coupling conditions, we consider first both SP and QE subsystems uncoupled. For this purpose, we solve Equation (1) numerically and compute the normalized zero-delay second-order correlation function in the steady state $g^{(2)}(0) = \langle \mathbf{E}_D^- \mathbf{E}_D^- \mathbf{E}_D^+ \mathbf{E}_D^+ \rangle / \langle \mathbf{E}_D^- \mathbf{E}_D^+ \rangle^2$. We only consider low laser intensities, and study quantum correlations far from the pumping regime in which QE saturation becomes relevant. Figure 2 plots $g^{(2)}(0)$ as a function of the laser detuning for an empty plasmonic cavity (black dash-dotted line) and ensembles of different number of emitters (color solid lines). The parameters modelling the single SP mode are: $\omega_{SP} = 3$ eV, $\gamma_{SP} = 0.1$ eV and $\mu_{SP} = 19$ e·nm [5]. Our calculations yield $g^{(2)}(0) = 1$, as expected from the SP inherent bosonic character. The QE parameters are: $\omega_{QE} = 3$ eV, $\gamma_{QE}^{r} = 6$ μeV ($\mu_{QE} = 1$ e·nm), and $\gamma_{QE}^{nr} = 15$ meV. These values correspond to low quantum yield QEs, accounting for the emission quenching that takes place in dense ensembles [3, 12]. For comparison, the correlation spectra for QEs with $\gamma_{QE}^{nr} = 0$ are also shown (color dashed lines). In all cases, photon statistics is sub-Poissonian ($g^{(2)}(0) < 1$), but the degree of antibunching decreases rapidly with the ensemble size. As N increases, the system bosonizes and the quantum character of the scattered light is lost (note that $g^{(2)}(0) = 0.96$ for $N = 50$). Neglecting nonradiative damping only leads to an extremely narrow Lorentzian-like profile, which suppresses antibunching exactly at zero detuning. Note that the $g^{(2)}(0)$ behaviour obtained from our model is in accordance with more sophisticated descriptions [19].

Exact numerical solutions to Equation (1) can be obtained for strong QE-SP coupling. However, such calculations are only possible for configurations involving very small QE ensembles [20], even far from the QE saturation regime [21]. In order to circumvent this limitation and explore photon statistics in mesoscopic ensembles, we map Equation (1) into an effective non-Hermitian Hamiltonian [22] of the form

$$\hat{H}_{\text{eff}} = \hat{H} - i\hbar\frac{\gamma_{SP}}{2}\hat{a}^\dagger\hat{a} - i\hbar\frac{\gamma_{QE}^{nr}}{2}\hat{S}_z - i\hbar\frac{\gamma_{QE}^{r}}{2}\hat{S}^+\hat{S}^- \quad (3)$$

where $\hat{H}$ is given by Equation (2). Note that $\hat{H}_{\text{eff}}$ depends only on the collective bright state operators of the QEs and is independent of the dark states of the ensemble (superpositions of QE excitations which do not couple to the plasmon or external light), which means a drastic reduction in the Hilbert space for large N. Equation (3) results from neglecting the so-called refilling or feeding terms $\hat{O}\rho\hat{O}^\dagger$ in the Lindblad super-operators in Equation (1). This approximate approach can be safely employed in the regime of low pumping, where the ground state (no excitations in the system) can be considered as a reservoir with population equal to 1. In this limit, we can solve the Schrödinger equation for $\hat{H}_{\text{eff}}$ treating the coherent driving, E_L, as a perturbative parameter [23].

As we are interested in intensity correlations, we can restrict our perturbative treatment of Equation (3) to second order and truncate the Hilbert space at the level of two excitations. This way, analytical expressions for the scattered intensity and the intensity correlations can be obtained. In the following, for simplicity, we also assume that the plasmonic near-field, $\mathbf{E}_{SP}$, is parallel to the laser field, $\mathbf{E}_L$ (as, for example, in particle-on-mirror cavities [15]). Moreover, we only consider the optimum configuration for strong coupling, in which $\boldsymbol{\mu}_{QE}$ is aligned with $\mathbf{E}_{SP}$. The scattering intensity, $I = \langle \mathbf{E}_D^- \mathbf{E}_D^+ \rangle$, is given within first-order perturbation theory as

$$I = (\eta N \mu_{SP} \Omega_{SP})^2 \left| \frac{\eta\tilde{\Delta}_{SP} + \tilde{\Delta}_{QE}/\eta N - 2\lambda}{\tilde{\Delta}_{SP}\tilde{\Delta}_{QE} - N\lambda^2} \right|^2, \quad (4)$$

where $\eta = \mu_{QE}/\mu_{SP} = \Omega_{QE}/\Omega_{SP}$, $\tilde{\Delta}_{SP} = \Delta_{SP} - i\gamma_{SP}/2$ and $\tilde{\Delta}_{QE} = \Delta_{QE} - i(\gamma_{QE}^{nr} + N\gamma_{QE}^{r})/2$. Using second-order perturbation theory, the correlation function, $g^{(2)}(0)$, can be expressed as

$$g^{(2)}(0) = \left| 1 - \frac{1}{N}\left(\frac{\eta\tilde{\Delta}_{SP} - \lambda}{\eta\tilde{\Delta}_{SP} + \tilde{\Delta}_{QE}/\eta N - 2\lambda} \right)^2 \frac{(\tilde{\Delta}_{QE} + iN\gamma_{QE}^{r}/2)[\tilde{\Delta}_{QE}\tilde{\Delta}_{SP} + (\tilde{\Delta}_{SP} - \lambda/\eta)^2 - N\lambda^2]}{(\tilde{\Delta}_{QE} + i\gamma_{QE}^{r}/2)[\tilde{\Delta}_{QE}\tilde{\Delta}_{SP} + \tilde{\Delta}_{SP}^2 - N\lambda^2] - 2\tilde{\Delta}_{SP}(N-1)\lambda^2} \right|^2. \quad (5)$$

Note that Equation (5) yields $g^{(2)}(0) = (1 - 1/N)^2$ at $\lambda = 0$ and $\eta \to \infty$, which recovers the flat correlation

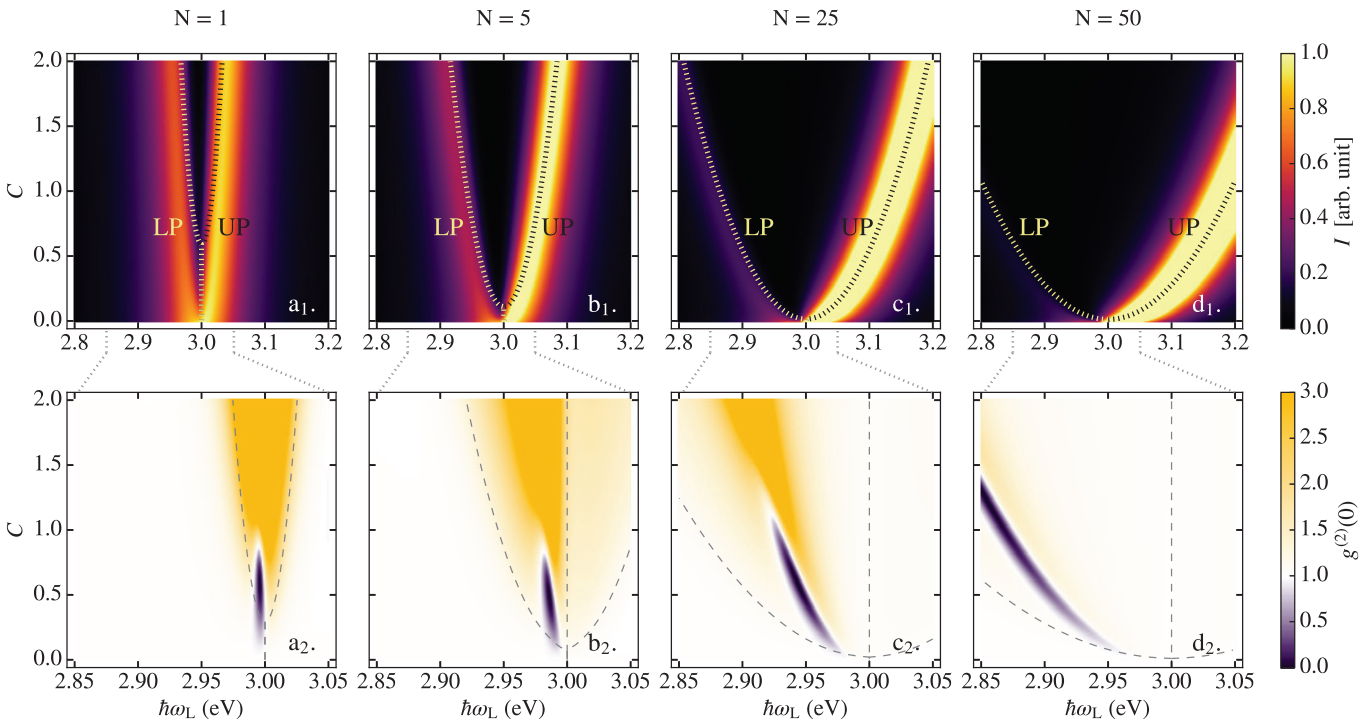

FIG. 3. Scattering intensity I (a_1-d_1) and zero-delay second-order correlation function $g^{(2)}(0)$ (a_2-d_2) versus laser frequency and single emitter cooperativity for various QE-SP systems. In the upper (lower) panels dotted (dashed) lines plot the PEP frequencies (half frequencies) in the one-excitation (two-excitation) manifold.

spectra in Figure 2 for low-quality-factor QE ensembles.

Figure 3 renders the far-field intensity (top row) and correlations (bottom row) for a nanocavity filled with four different QE ensembles: $N = 1$ (a), 5 (b), 25 (c) and 50 (d). The horizontal and vertical axes correspond to laser frequency and QE-SP coupling strength, respectively. The latter is expressed through the single-emitter cooperativity, $C = 2\lambda^2/\gamma_{\rm QE}\gamma_{\rm SP}$, with upper limit $C = 2$ ($\lambda = 0.03$ eV), well below the collective ultra-strong coupling regime. We restrict our attention to QE-SP resonant coupling and consider the same parameters as in Figure 2. Although the quantitative results shown in Figure 3 depend on the specifics of the system, we have checked that our findings and their fundamental implications remain valid for a wide range of realistic configurations.

The complex $g^{(2)}(0)$ patterns in Figure 3(a_2)-(d_2) reveal that both photon bunching and antibunching take place in the strong coupling regime. These panels also show that the main quantum statistical features emerging at the single-emitter level (which are in qualitative agreement with recent experimental reports on semiconductor cavities [24, 25]) are mostly retained as N increases. Up to $N \sim 25$, photon emission is antibunched within a narrow frequency window located at $C \lesssim 1$, which implies that the single-emitter cooperativity can be considered as the key parameter determining photon correlations in ensembles containing up to several tens of QEs. Note that for very large N, antibunching is also observed for larger C-values. On the other hand, bunched emission takes place at larger coupling strengths and within broader spectral domains for all N. Remarkably, there are spectral windows in which strong antibunching ($g^{(2)}(0) \approx 0$) takes place even for $N = 50$, whereas the emission from the uncoupled QE ensemble is essentially classical (see Figure 2). This is the main result of this Letter, namely that in comparison to the uncoupled subsystems, collective plasmonic strong coupling can significantly enhance photon correlations in mesoscopic PEP systems.

By taking advantage of our analytical approach, we can gain physical insight into the results shown in Figure 3. The intensity maps present two scattering maxima, whose origin lies at the denominator of Equation (4). Its vanishing condition yields analytical expressions for the dispersion of the lower (LP) and upper (UP) PEPs in the first rung (one-excitation manifold) of the Tavis-Cummings ladder. These PEP frequencies, which naturally incorporate the $\sqrt{N}$ scaling characteristic of collective strong coupling, are plotted in dotted lines in all top panels. Note that the intensity maxima overlap with the PEP dispersion bands except for $N = 1$ and $C \lesssim 0.5$. This region, also perceptible for $N = 5$ at lower C, falls within the weak coupling regime, where Fano-like interferences between SP and QE emission gives rise to sharp scattering dips [26]. As N increases, the contrast between UP (brighter) and LP (darker) scattering peaks increases. By introducing the PEP frequencies in the numerator of Equation (4), the origin of this asymmetry becomes clear. Neglecting QE and SP damping, we obtain

$I \propto (1 \mp \sqrt{N}\eta)^2$, where the upper (lower) sign must be used for LP (UP). Thus, QE and SP dipole moments are antiparallel along the LP dispersion, which diminishes I as N approaches $1/\eta^2$.

In a similar way as in the scattered intensity, we can expect that the vanishing of the denominator in the second term of Equation (5) could give rise to nonclassical light. At $N = 1$, the resonant frequencies emerging from this condition are equal to half the energies of the LP (upper sign) and UP (lower sign) in the second rung of the Jaynes-Cummings ladder [27]. For $N > 1$, the same condition leads to a cubic equation, as it accounts for the emergence of the middle PEPs in the two-excitation manifold (whose real half-frequency is equal to $\omega_{\mathrm{QE/SP}}$). Moreover, notice the presence of the numerator of Equation (4) in the denominator of the first factor in Equation (5). As discussed above, this term acquires the form $(1 - \sqrt{N}\eta)$ at the LP band. Therefore, we can infer that the darker character of LPs also makes them more suitable for photon correlations. PEP half-frequencies in the two-excitation manifold are plotted in dashed lines in Figure 3(a_2)-(d_2). The regions of strong photon correlations do not occur exactly at one of the polariton energies, but slightly above the LP dispersion. This indicates that photon correlations, i.e., significant deviations from $g^{(2)}(0) = 1$, do not originate from transitions along a single PEP ladder, but from the interference in the emission involving different hybrid states. This underlines the crucial role that strong coupling plays: While each PEP by itself is quasi-bosonic, the hybridization achieved through strong coupling not only manifests in their mixed light-matter character, but also ensures the coexistence of multiple PEP modes separated by the Rabi splitting. It is only the interference between the emission from these different but closely related modes that leads to strongly nonclassical light emission.

In order to obtain a general view on the degree of bunching and antibunching attainable through QE-SP coupling, we evaluate Equation (5) at its spectral maxima and minima. Figure 4 explore these extreme $g^{(2)}(0)$ values as a function of cooperativity and number of emitters. The inset renders overlapping maps for $\mathrm{Max}[g^{(2)}(0)]$ (yellow) and $\mathrm{Min}[g^{(2)}(0)]$ (violet), and the top and bottom panels plot cuts of these maps for various C-values. We can identify three domains according to the statistics of the scattered photons. For small QE ensembles and large C, only positive correlations take place, as in Figure 3(a_2)-(c_2) for $C > 1$. In this regime, $\mathrm{Max}[g^{(2)}(0)]$ grows with increasing coupling strength and develops a maximum at $N \sim 10$ for all C. For very large N, a second domain is apparent. In this limit, PEPs bosonize as the $1/N$ factor in Equation (5) governs $g^{(2)}(0)$, yielding maxima and minima approaching 1 monotonically as the number of QEs increases. Both bunched and antibunched emission takes place (within different spectral windows) at intermediate N and C. In this third domain, positive correlations decay monotonically with N, whereas negative correlations are enhanced. $\mathrm{Min}[g^{(2)}(0)]$ diminishes and reaches a minimum value, which corresponds to the lowest $g^{(2)}(0)$ achievable for a given N and any C (or *vice versa*). It can be proven that this minimum coincides with a sharp dip in the population of the plasmon state (written as a linear combination of PEPs) in the two-excitation manifold. In the limit of vanishing η (which is a good approximation for our problem at small N), this condition simplifies to $C = \frac{\gamma_{\mathrm{QE}}+\gamma_{\mathrm{SP}}}{2\gamma_{\mathrm{SP}}} \simeq \frac{1}{2}$. Figure 4(bottom) shows this minimum developing with increasing cooperativity at $N \sim 10$ and reaching $g^{(2)}(0) = 0$ at $C = 0.5$. Remarkably, this zero in $g^{(2)}(0)$ shifts to larger N for higher cooperativity, yielding strong photon antibunching at ensemble sizes as large as 100 QEs. Therefore, as anticipated in Figure 3(d_2), plasmonic strong coupling leads to the emergence of quantum nonlinearities in large excitonic systems, which would present $g^{(2)}(0) \simeq 1$ when they are not coupled to the plasmonic nanocavity.

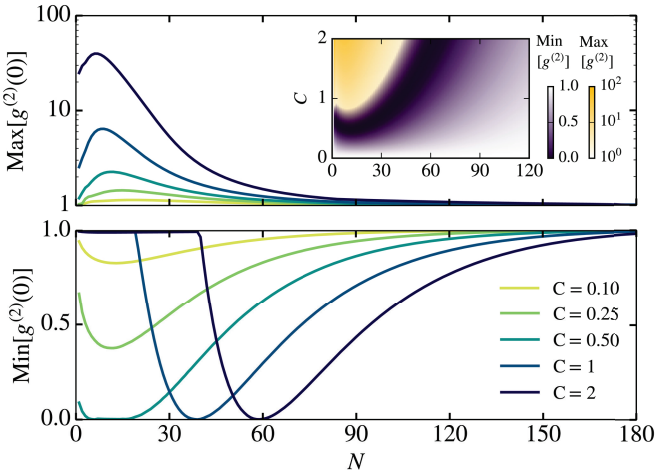

FIG. 4. Maximum (top) and minimum (bottom) correlation function as a function of the QE ensemble size for several values of the single emitter cooperativity. The inset in the upper panel show the map of photon positive (yellow) and negative (violet) correlations as a function of N and C.

To conclude, we have investigated the complex photon statistics phenomenology that emerges from the strong coupling of a mesoscopic ensemble of quantum emitters and a single plasmon mode supported by a generic nanocavity. We have presented an analytical method describing the optical response of these systems under low-intensity coherent illumination. Our approach provides insights into the role that both the plasmon-exciton-polariton ladder and its tuning through the single emitter cooperativity play in the emission of strongly correlated (bunched and/or antibunched) light. Finally, our results demonstrate the robustness of these compound systems against bosonization effects, predicting strong intensity correlations at considerable ensemble sizes. Our theoretical findings demonstrate the feasibility and establish experimental guidelines towards the realisation of nanoscale nonclassical light sources operating beyond the single-emitter level.

This work has been funded by the European Research Council under Grant Agreement ERC-2011-AdG 290981, the EU Seventh Framework Programme (FP7-PEOPLE-2013-CIG-630996 and FP7-PEOPLE-2013-CIG-618229), and the Spanish MINECO under contracts MAT2014-53432-C5-5-R and FIS2015-64951-R, as well as through the "María de Maeztu" programme for Units of Excellence in R&D (MDM-2014-0377).

* a.fernandez-dominguez@uam.es
† fj.garcia@uam.es

[1] P. Törmä and W. L. Barnes, Rep. Prog. Phys. **78**, 013901 (2015).
[2] J. Bellessa, C. Bonnand, J. C. Plenet, and J. Mugnier, Phys. Rev. Lett. **93**, 036404 (2004).
[3] T. Schwartz, J. A. Hutchison, C. Genet, and T. W. Ebbesen, Phys. Rev. Lett. **106**, 196405 (2011).
[4] A. González-Tudela, P. A. Huidobro, L. Martín-Moreno, C. Tejedor, and F. J. García-Vidal, Phys. Rev. Lett. **110**, 126801 (2013).
[5] A. Delga, J. Feist, J. Bravo-Abad, and F. J. García-Vidal, Phys. Rev. Lett. **112**, 253601 (2014).
[6] G. Zengin, M. Wersäll, S. Nilsson, T. J. Antosiewicz, M. Käll, and T. Shegai, Phys. Rev. Lett. **114**, 157401 (2015).
[7] F. Todisco, S. D'Agostino, M. Esposito, A. I. Fernández-Domínguez, M. De Giorgi, D. Ballarini, L. Dominici, I. Tarantini, M. Cuscuna, F. Della Sala, G. Gigli, and D. Sanvitto, ACS Nano **9**, 9691 (2015).
[8] J. A. Hutchison, T. Schwartz, C. Genet, E. Devaux, and T. W. Ebbesen, Angew. Chem. **124**, 1624 (2012).
[9] J. Galego, F. J. García-Vidal, and J. Feist, Phys. Rev. X **5**, 041022 (2015).
[10] E. Orgiu, J. George, J. A. Hutchison, E. Devaux, J. F. Dayen, B. Doudin, F. Stellacci, C. Genet, J. Schachenmayer, C. Genes, G. Pupillo, P. Samorì, and T. W. Ebbesen, Nat. Materials **14**, 1123 (2015).
[11] J. Feist and F. J. García-Vidal Phys. Rev. Lett. **114**, 196402 (2015).
[12] M. Ramezani, A. Halpin, A. I. Fernández-Domínguez, J. Feist, S. R.-K. Rodriguez, F. J. García-Vidal, and J. Gómez-Rivas, Optica **4**, 31 (2017).
[13] M. S. Tame, K. R. McEnery, S. K. Özdemir, J. Lee, S. A. Maier, and M. S. Kim, Nat. Physics **9**, 329 (2013).
[14] T. Holstein and H. Primakoff, Phys. Rev. **58**, 1098 (1940).
[15] R. Chikkaraddy, B. de Nijs, F. Benz, S. J. Barrow, O. A. Scherman, E. Rosta, A. Demetriadou, P. Fox, O. Hess, and J. J. Baumberg, Nature **535**, 127 (2016).
[16] K. Santhosh, O. Bitton, L. Chuntonov, and G. Haran, Nat. Comm. **7**, 11823 (2016).
[17] R.-Q. Li, D. Hernangómez-Pérez, F. J. García-Vidal, and A. I. Fernández-Domínguez, Phys. Rev. Lett. **117**, 107401 (2016).
[18] M. Tavis and F. W. Cummings, Phys. Rev. **170**, 379 (1968).
[19] F. Miftasani, and P. Machnikowski, Phys. Rev. B **93**, 075311 (2016).
[20] A. Auffeves, D. Gerace, S. Portolan, A. Drezet, and M. França Santos, New J. Phys. **13**, 093020 (2011).
[21] A. N. Poddubny, M. M. Glazov, and N. S. Averkiev, Phys. Rev. B **82**, 205330 (2010).
[22] P. M. Visser and G. Nienhuis, Phys. Rev. A **52**, 4727 (1995).
[23] R. J. Brecha, P. R. Rice, and M. Xiao, Phys. Rev. A **59**, 2392 (1999).
[24] K. Müller, A. Rundquist, K. A. Fisher, T. Sarmiento, K. G. Lagoudakis, Y. A. Kelaita, C. Sánchez-Muñoz, E. del Valle, F. P. Laussy, and J. Vučović, Phys. Rev. Lett. **114**, 233601 (2015).
[25] A. Faraon, I. Fushman, D. Englund, N. Stoltz, P. Petroff, and J. Vučović, Nat. Phys. **8**, 859 (2008).
[26] A. Ridolfo, O. Di Stefano, N. Fina, R. Saija, and S. Savasta, Phys. Rev. Lett. **105**, 263601 (2010).
[27] F. P. Laussy, E. del Valle, M. Schrapp, A. Laucht, and J. J. Finley, J. Nanophot. **6**, 061803 (2012).
[28] A. Kubanek, A. Ourjoumtsev, I. Schuster, M. Koch, P.W. H. Pinkse, K. Murr, and G. Rempe, Phys. Rev. Lett. **101** 203602 (2008).